



High-Throughput Analysis of Arabidopsis Stem Vibrations to Identify Mutants With Altered Mechanical Properties

Miyuki T. Nakata¹, Masahiro Takahara², Shingo Sakamoto¹, Kouki Yoshida³ and Nobutaka Mitsuda^{1*}

¹ Plant Gene Regulation Research Group, Bioproduction Research Institute, National Institute of Advanced Industrial Science and Technology, Tsukuba, Japan, ² Acacia Horticulture, Adachi, Japan, ³ Technology Center, Taisei Corporation, Yokohama, Japan

OPEN ACCESS

Edited by:

Takumi Higaki,
Kumamoto University, Japan

Reviewed by:

Yoichiroh Hosokawa,
Nara Institute of Science and
Technology (NAIST), Japan
Darshil U. Shah,
University of Cambridge,
United Kingdom

*Correspondence:

Nobutaka Mitsuda
nobutaka.mitsuda@aist.go.jp

Specialty section:

This article was submitted to
Technical Advances in Plant Science,
a section of the journal
Frontiers in Plant Science

Received: 20 February 2018

Accepted: 22 May 2018

Published: 12 June 2018

Citation:

Nakata MT, Takahara M, Sakamoto S,
Yoshida K and Mitsuda N (2018)
High-Throughput Analysis of
Arabidopsis Stem Vibrations to Identify
Mutants With Altered Mechanical
Properties. *Front. Plant Sci.* 9:780.
doi: 10.3389/fpls.2018.00780

Mechanical properties are rarely used as quantitative indices for the large-scale mutant screening of plants, even in the model plant *Arabidopsis thaliana*. The mechanical properties of plant stems generally influence their vibrational characteristics. Here, we developed Python-based software, named AraVib, for the high-throughput analysis of free vibrations of plant stems, focusing specifically on Arabidopsis stem vibrations, and its extended version, named AraVibS, to identify mutants with altered mechanical properties. These programs can be used without knowledge of Python and require only an inexpensive handmade setting stand and an iPhone/iPad with a high-speed shooting function for data acquisition. Using our system, we identified an *nst1 nst3* double-mutant lacking secondary cell walls in fiber cells and a *wrky12* mutant displaying ectopic formation of secondary cell wall compared with wild type by employing only two growth traits (stem height and fresh weight) in addition to videos of stem vibrations. Furthermore, we calculated the logarithmic decrement, the damping ratio, the natural frequency and the stiffness based on the spring-mass-damper model from the video data using AraVib. The stiffness was estimated to be drastically decreased in *nst1 nst3*, which agreed with previous tensile test results. However, in *wrky12*, the stiffness was significantly increased. These results demonstrate the effectiveness of our new system. Because our method can be applied in a high-throughput manner, it can be used to screen for mutants with altered mechanical properties.

Keywords: Arabidopsis, AraVib, Python, free vibration, damped natural frequency, mechanical properties, *nst1 nst3*, *wrky12*

INTRODUCTION

Lignocellulosic biomass, which comes mainly from plant cell walls, is one of the largest renewable resources, which are indispensable for human society. It has an extremely broad range of uses, including in fuels, paper, building materials, furniture, crafts, biochemicals, biomaterials, and acoustic instruments. Consequently, its production and the selection of plant species with high-yield/quality lignocellulose levels are being actively studied. Lignocellulosic biomass consists mainly of cellulose, hemicellulose, and lignin, which are high-molecular weight polymers that interact with

each other in a complex manner, making lignocellulose highly recalcitrant. While primary cell walls exist in all plant cells, thickened secondary cell walls are preferentially formed in vessel and fiber cells to confer hydrophobicity and robustness to tissues, contribute to the transport of water and nutrients, support plant bodies and prevent pathogen invasion. Because the secondary cell walls form a large proportion of the plant biomass, their recalcitrance to degradation could be a focus of molecular and traditional breeding.

In model plants, the large-scale screening of various mutants and transformed strains in which lignocellulose could be modified has been attempted. In particular, *Arabidopsis thaliana* is often used as the model plant because it has many advantages, such as a short-generation period, and the feasibility of genetic engineering and forward genetic screening. In a phenotypic screening, anatomical changes, biomass and the cellulose saccharification efficiency have been mainly used as indices (Santoro et al., 2010; Wang et al., 2010; Cassan-Wang et al., 2013; Sakamoto and Mitsuda, 2015). However, even though the mechanical properties of the stem are important in physiological studies and applications, their evaluation in a large-scale screening usually relies on primitive and qualitative methods, such as visual observations and hand-bending tests. However, other mechanical tests, such as tensile, compression and mechanical bending tests (Gibson, 2012), can be applied to *A. thaliana* (Ryden et al., 2003; MacMillan et al., 2013; Brulé et al., 2016; Sakamoto et al., 2016). Micro-mechanical or micro-tensile tests combining deformations and monitoring have also been established (Mott et al., 1996; Köhler and Spatz, 2002). The methods for investigating the strength of stem in cellular and/or cell-wall level, as well as tissue level, are available. Additionally, in recent years, a method measuring local mechanical properties using an atomic force microscope has been developed (Peaucelle et al., 2011; Fernandes et al., 2012; Radotić et al., 2012; Braybrook and Peaucelle, 2013; Peaucelle, 2014). However, these assays are not commonly used for screening because they require expensive and specialized stationary instruments. To find useful genes and mutations with high industrial values, the mechanical properties of the stems could be important indices. Thus, the development of a high-throughput and low-cost quantitative screening method is required.

In this study, we focused on the stem's vibrational frequency as an indicator of its mechanical properties. Vibration is a general physical phenomenon observed when an object is deformed by an external force. Every object has its own vibrational frequency, which depends on its own stiffness and mass. In fact, vibrational characteristics are used for evaluating mechanical properties in various plants, and various methods for measuring vibration have been proposed. For instance in wood, hitting it with a hammer and analyzing sound waves is generally used for calculating the mechanical properties (Yamamoto et al., 1980; Halabe et al.,

1997). Additionally, the resonance method also has been used to examine the mechanical properties of plant tissues (Virgin, 1955; Falk et al., 1958; Burström et al., 1967, 1970; Uhrström, 1969; Burström, 1971; Cosgrove and Green, 1979; Finney and Abbott, 1979; Uhrström and Svensson, 1979; Niklas and Moon, 1988). The flexural rigidity of the stem has been evaluated using free vibrations (Zebrowski, 1991; Spatz and Speck, 2002). Even in *A. thaliana*, a modal analysis of stem vibration was attempted (Der Loughian et al., 2014), and the possibility of a nondestructive phenotyping method was proposed (Shah et al., 2017). However, these studies aimed to calculate physical property values but did not intend to apply them to the large-scale screening of mutants with altered mechanical properties.

In this research, to promote the application of vibrational analyses in the field of molecular genetics using *A. thaliana*, we developed Python-based software for the high-throughput analysis of Arabidopsis stem vibrations (named AraVib) and an extended version, named AraVibS, to identify Arabidopsis mutants with altered mechanical properties. The software are free of charge and can be used without any knowledge of Python. For data acquisition, we have established a method to analyze the free vibration of the inflorescence stems of *A. thaliana*. Here, we demonstrate that our system can rapidly estimate the mechanical properties of stems and discriminate mutants having altered cell walls.

MATERIALS AND METHODS

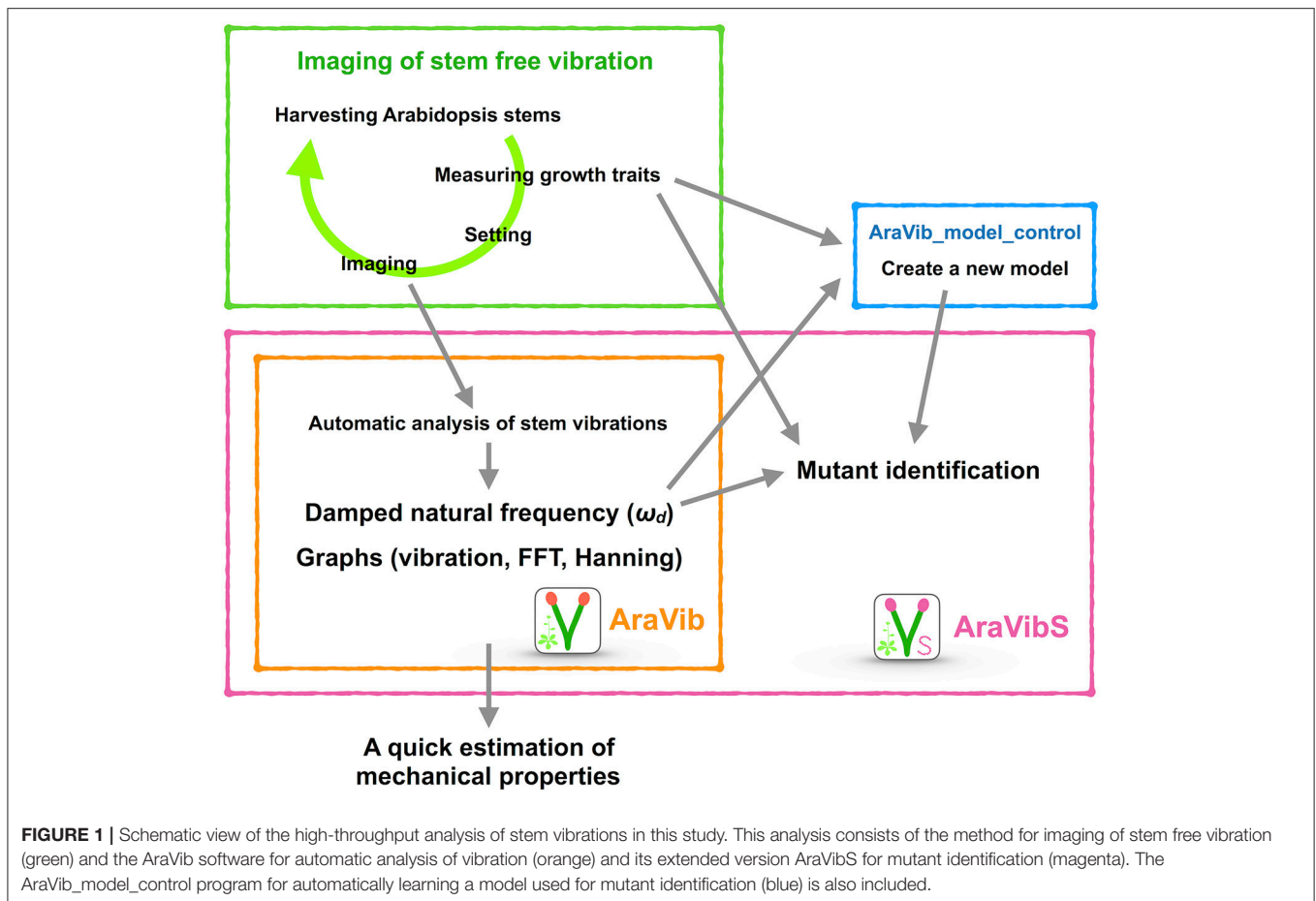
Plant Strains and Growth Conditions

A. thaliana accession Columbia-0 was used as the wild type. The *nst1-1 nst3-1* double mutant, which has defects in secondary cell wall formation in fiber cells of the inflorescence stem (Mitsuda et al., 2007; Zhong et al., 2007), was described in Mitsuda et al. (2007). The *wrky12-1* mutant, in which the deposition of secondary cell wall components were ectopically observed in the pith cells, was described in Wang et al. (2010). The seeds were rinsed in a Plant Preservative Mixture solution (3% Plant Preservative Mixture and 0.1% Triton-X 100; Nacalai Tesque Inc., Kyoto, Japan), sown on a culture soil (soil mix:vermiculite, 1:1) and cultivated for ~1.5–2 months under long-day conditions (16-h light/8-h dark) at 22°C. In experimental condition 1, multiple plants were grown in the same plant pot, and the area per plant was 1,200 mm² or less. In experimental condition 2, plants were grown individually in ARASystem (<http://www.arasystem.com/>), and the area per plant was ~2,000 mm².

Imaging of Stem Vibrations

Our method consists of three sections: measuring growth traits, settings and imaging (Figures 1, 2) after harvesting the stem. First, we measured growth traits, including the stem height (H) and 10-cm stem fresh weight (FW). H was measured with a ruler. To reduce the effect of non-uniformity in weight distribution, the basal part of the stem was trimmed to a length of 10 cm with scissors, and all accessories, such as leaves, branches, flowers and fruits, were removed. The FW was weighed with a precision balance. Second, we set the 10-cm stem sample. The 1-cm position at the base was marked with a black marker,

Abbreviations: ω_d , the damped natural frequency; δ , the logarithmic decrement; ζ , the damping ratio; ω_n , the natural frequency; c , the damping coefficient; k , the stiffness; m_{eq} , the equivalent mass of the oscillator; FW, the fresh weight of the trimmed stem; AIR, the alcohol-insoluble residues of the trimmed stem; H, stem height; FFT, Fast Fourier Transform.



and the apical end of the stem was marked with red marker. To ensure detection by AraVib, a large enough amount of the red marker should be applied. The weight of the applied red marker itself was 1% or less of tested stems and, therefore ignorable. The 1-cm stem section below the black mark was sandwiched between plastic boards and firmly fixed with a rubber band and then placed on a plastic box (termed “a handmade setting board”). The plastic boards and the plastic box were made from refill attachments for 250- μ L pipette tips (RAININ: GPS-250S). The background was covered with a black cloth or cardboard. The iPad/iPhone camera was fixed at a position 20 cm away from the stem. Third, we imaged stem vibrations. To apply linear bending, the upper position of the stem (3–4 cm from the tip) was grasped by tweezers and pulled sideways at an angle without breaking the stem. Immediately after the shooting had started, the stem was released (Supplementary Movies 1, 2). The image of the stem vibration was captured for 3–4 s with the high-speed shooting function (240 fps) of iPad/iPhone video. These procedures were repeated for each sample. Because the time from the measurement of the stem length to the end of capturing the vibration is within 2–3 min per sample (Figure 2), the change in FW resulting from a loss of moisture during the experimental process should be small.

Development of AraVib and AraVibS

AraVib is a command-line software that automatically analyzes the stem vibration movies, which were recorded using the above-mentioned method, in a batch (Figures 1, 3). In AraVib, the red marker on the black background is tracked, the centroid coordinates of the marker are determined, and the coordinates are converted to displacement data. The displacement data are then multiplied by the Hanning window (Harris, 1978), and the Hanning-multiplied data are used to calculate the damped natural frequency (ω_d), using Fast Fourier Transform (FFT). Details of the algorithms and their optimization procedures for AraVib can be found in the Supplementary Materials and Supplementary Figures 1–3. In this study, AraVib was run on the MacBook Pro (2.4 GHz Intel Core i7, 8GB 1600 MHz DDR3, macOS Sierra).

The latest version of the compressed AraVib folder containing these programs and some sample files is available in the GitHub page of AraVib. Details on how to use these programs are also available. The free Python packages or libraries, which are used in AraVib and AraVibS, are the OpenCV-Python package, NumPy package, the Python Pandas package, SciPy library, the pyplot package of the Matplotlib and Scikit-learn package. Details on how to set up them are shown in Supplementary Materials.

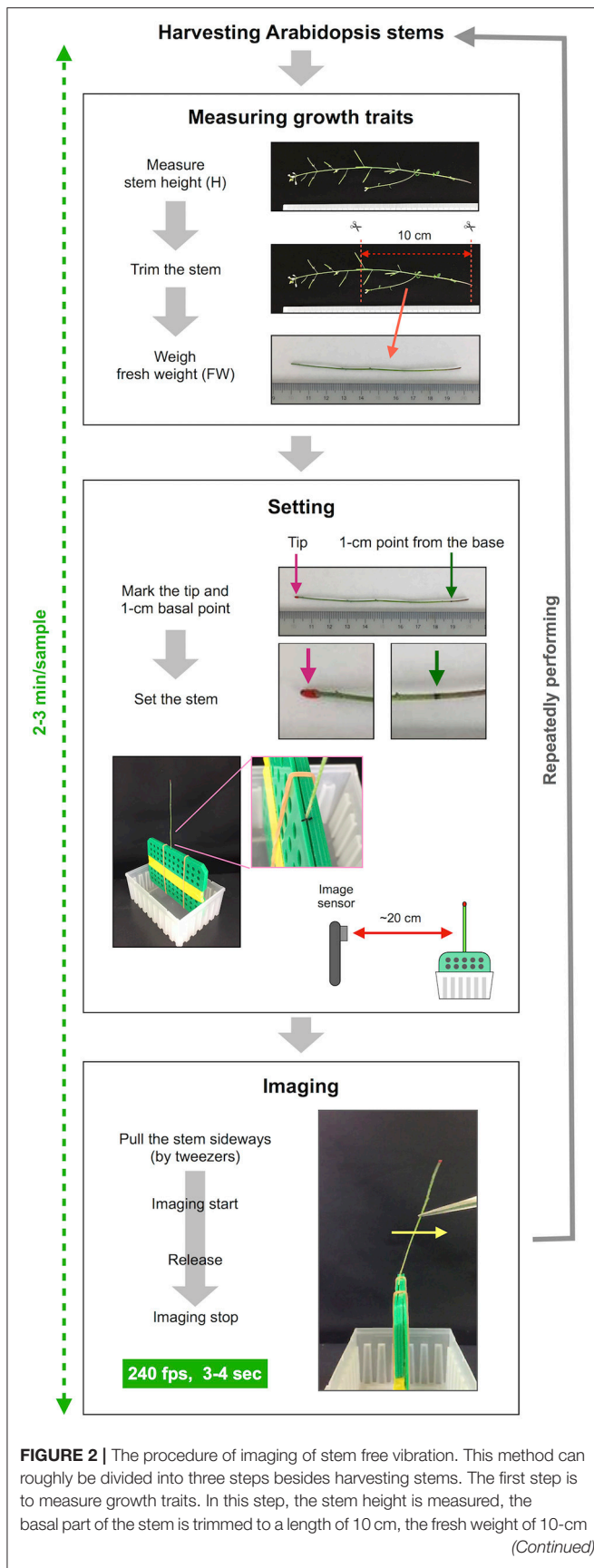


FIGURE 2 | stem is weighed. The second step is setting the stem sample. In this step, the trimmed stem is marked and set to the setting board. The setting board with the stem is placed ~20 cm from the image sensor of the iPhone/iPad. The third step is imaging. The stems are pulled sideways by tweezers, retained and released after imaging has started. Stem vibration is imaged in the slow-motion mode at 240 fps for 3–4 s. This series of procedures is repeated for each sample.

The analytical flow of AraVib is shown in **Figure 3A**. The output is the csv file of the ω_d list (**Figure 3A**) and three graphs of each sample, including the raw vibration waveform (**Figure 3B** and Supplementary Figure 4). AraVibS is an extended version of AraVib for the efficient detection of mutants using the ω_d data, which was calculated by AraVib, and growth traits (**Figure 1**). In addition, the AraVib_model_control program that assists in creating a model for mutant detection by AraVibS is included (**Figure 1**). **Figure 3A** shows the structure of the expanded AraVib folder.

The calculated ω_d is used for the analysis by itself (**Figures 4A–C, 5A,B**) and for the analysis combined with growth traits (**Figures 5C,D** and Supplementary Figures 5–7). Because the distribution of the combination of ω_d and growth traits is different between wild type and tested cell-wall mutants (**Figures 5C,D**), we developed an extended version of AraVib for mutant detection and named it AraVibS (**Figures 6A–C**). To detect mutants, a multiple linear regression model and fitting to the normal distribution are used in this program (**Figures 6A,B**). To easily optimize the model under each condition, we also developed the AraVib_model_control program that assists in creating a learned model and in calculating parameters fitted to the normal distribution (**Figures 6B,C**).

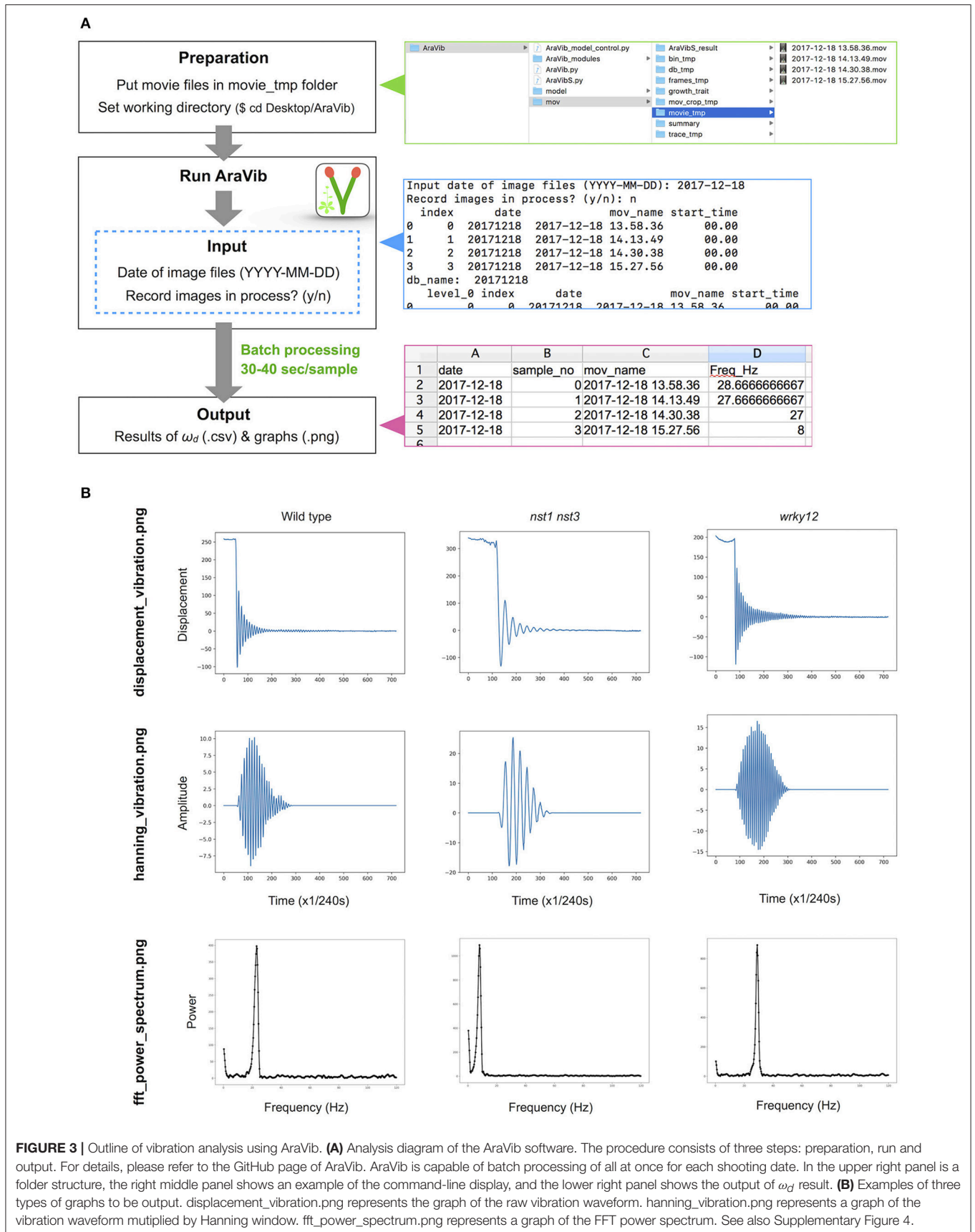
Equations for Estimating Mechanical Properties

By assuming that the stem is a simple spring-mass-damper system (**Figure 7A**), stiffness k and damping coefficient c can be estimated from ω_d and logarithmic decrement (Zebrowski, 1999; Villibor et al., 2016; **Figure 7B**; δ). According to Zebrowski (1999) in tapered stems of Triticale and Triticum, the dynamic behaviors of the vertical columns were different from those of the horizontal beams. However, the difference was very small when only 20 cm of the basal portion was used or when the tip load was very light (Zebrowski, 1999). Therefore, we concluded that this model could be applied to the estimation of mechanical properties when the non-tapered part of the stem is used and the tip weight is close to zero.

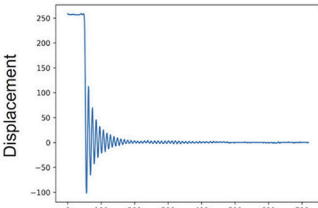
The δ -value was calculated from the maximum peak amplitude in each period in the graph of the raw vibration waveform (Zebrowski, 1999; de Silva, 2006; **Figure 7C**), as follows:

$$\delta = \frac{1}{r} \ln \left(\frac{A_i}{A_{i+r}} \right), \quad (1)$$

where A_i and A_{i+r} represent the maximum amplitudes of the i and $i+r$ periods, respectively. The peak amplitude in

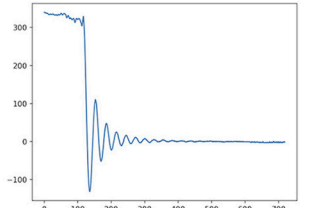


Wild type

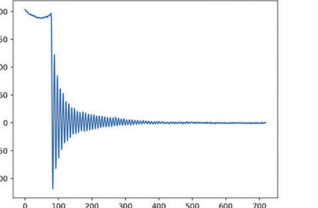


displacement_vibration.png

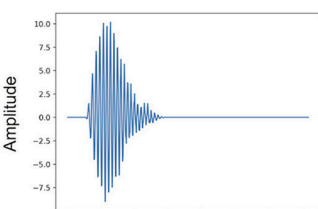
nst1 nst3

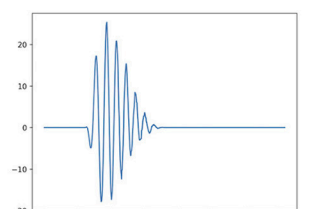


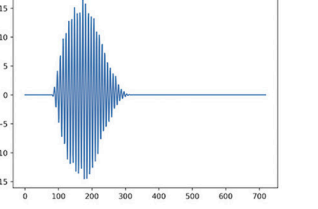
wrky12



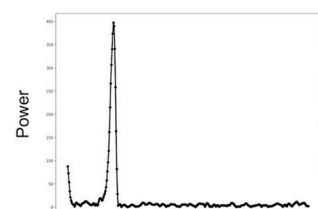
hanning_vibration.png

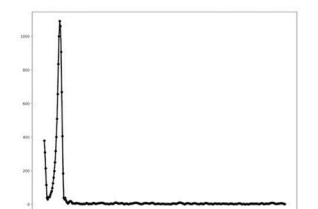


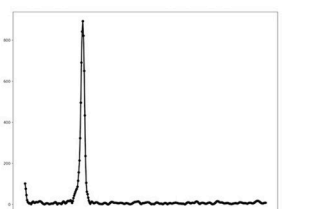




fft_power_spectrum.png







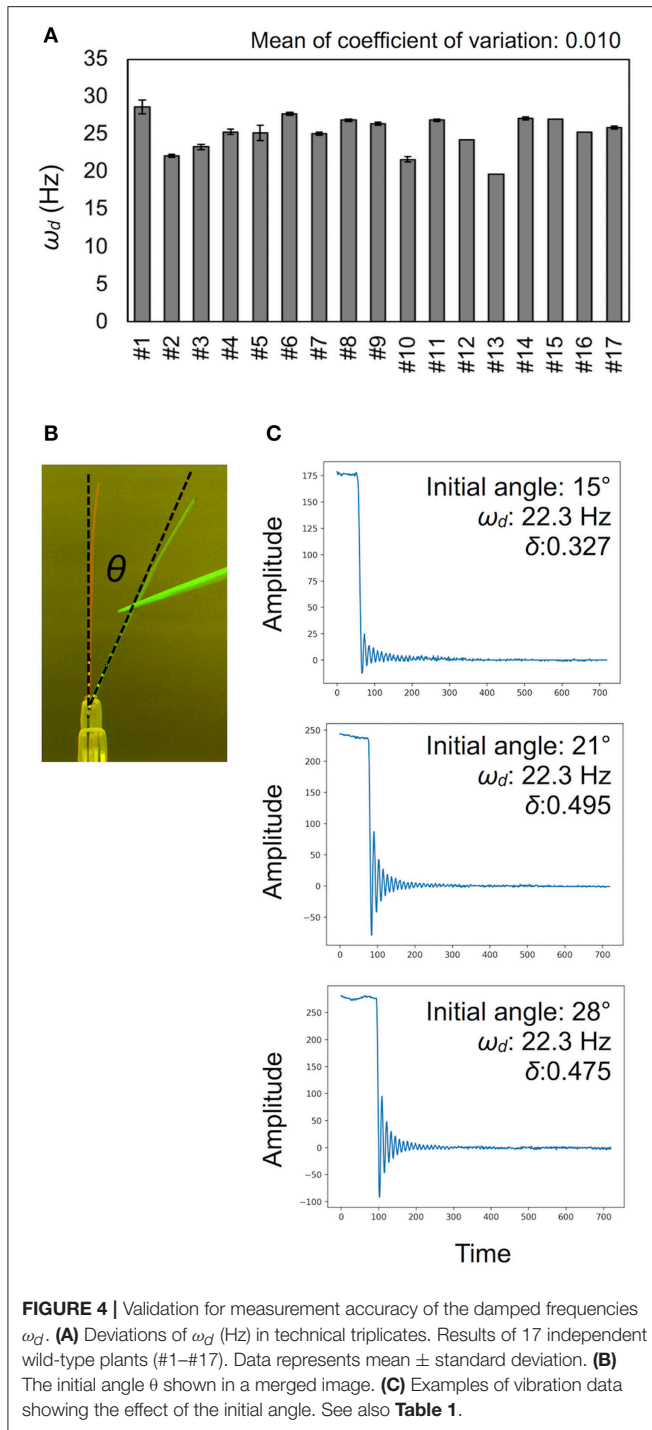


FIGURE 4 | Validation for measurement accuracy of the damped frequencies ω_d . **(A)** Deviations of ω_d (Hz) in technical triplicates. Results of 17 independent wild-type plants (#1–#17). Data represents mean \pm standard deviation. **(B)** The initial angle θ shown in a merged image. **(C)** Examples of vibration data showing the effect of the initial angle. See also **Table 1**.

each period was obtained by another program to automatically detect the maximum peaks from a graph of vibration data without Hanning-window processing. δ was estimated by a linear regression using multiple peak values to alleviate the influence of measurement errors. The pixel values of the peaks were natural log transformed and plotted for each peak number (**Figure 7C**). A linear regression was performed on four possible

consecutive data points from the first to ninth peaks, and the slope, r^2 , p -values were calculated. Among the calculated regression formulae, the absolute value of the slope of the regression equation where r^2 was maximum and the p -value was < 0.05 was adopted as δ (Supplementary Table 1). After calculation, the graphs of logarithmic plots of the pixel values of the peaks and the regression lines were visually confirmed. For samples with peak values that did not monotonically decrease or fit to the regression line, manual detection was performed using ImageJ (Abràmoff et al., 2004), and then, δ was calculated.

Based on two previous reports (Zebrowski, 1999; Villibor et al., 2016), the damping ratio (ζ), the natural frequency (ω_n), the damping coefficient (c) and the stiffness (k) were estimated from ω_d and δ (**Figure 7B**), as shown below.

ζ was estimated by the following equation.

$$\zeta = \frac{\delta}{\sqrt{(2\pi)^2 + \delta^2}} \quad (2)$$

ω_n was estimated by the following equation.

$$\omega_n = \frac{\omega_d}{\sqrt{1 - \zeta^2}} \quad (3)$$

c was estimated by the following equation.

$$c = 4\pi\omega_n m_{eq}\zeta \quad (4)$$

where m_{eq} represents the equivalent mass of the oscillator (**Figure 7A**). m_{eq} is expressed by the following equation as described in Zebrowski (1999):

$$m_{eq} = \alpha m_b + M, \quad (5)$$

where M represents the mass of the attached tip-point weight, but in our system this is substantially zero (see the following section). Also, m_b represents the weight of the beam; $\alpha = 0.245$ in the case of a beam showing a uniform weight distribution. The basal stem portion (10 cm from the base) of *A. thaliana* inflorescences without any accessories showed a uniform weight distribution on average (Supplementary Figure 8). Of the 10-cm stems, 1 cm was used to fix to the setting board (see the following section). Thus, the remaining 9-cm section contributed to the vibration. Thus,

$$m_{eq} = 0.245 \times 0.9 \times \text{FW}, \quad (6)$$

where FW represents the fresh weight of the 10-cm stem. The relationship between the natural frequency and the stiffness k was expressed by the following equation.

$$\omega_n = \frac{1}{2\pi} \sqrt{\frac{k}{m_{eq}}} \quad (7)$$

Thus, the stiffness k was estimated by the following equation.

$$k = (2\pi\omega_n)^2 m_{eq} \quad (8)$$

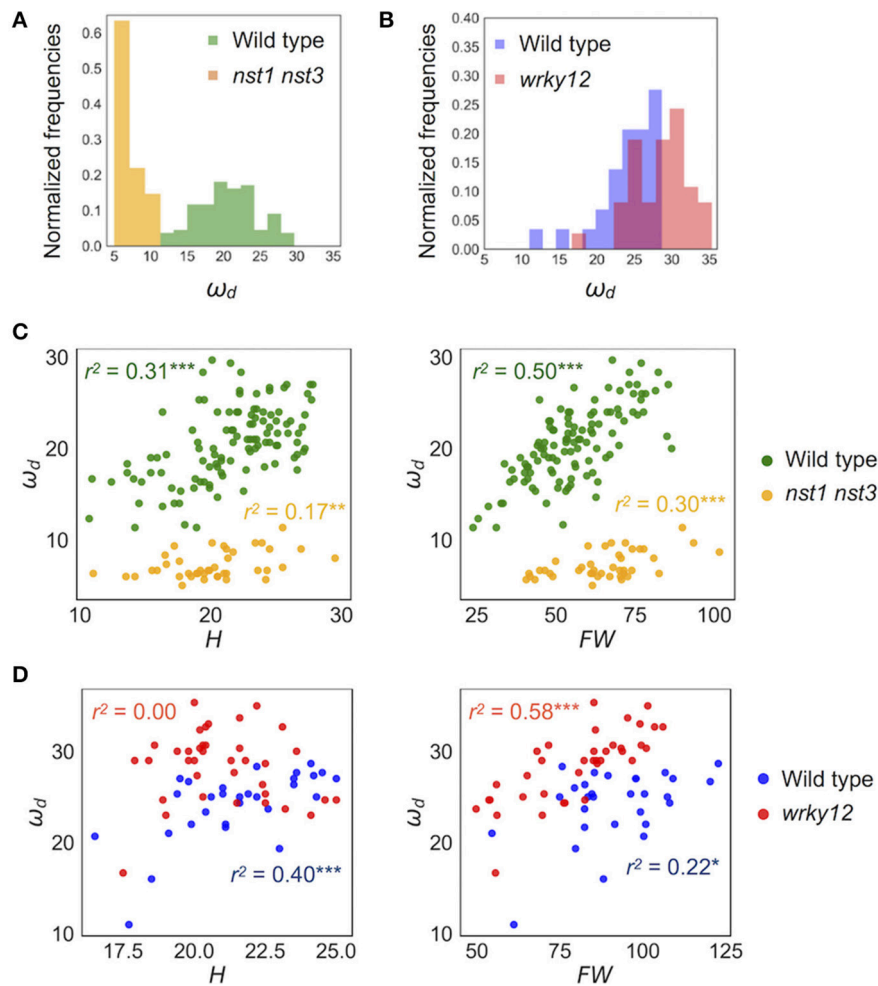


FIGURE 5 | Distribution of ω_d of wild type and cell-wall mutants. **(A,B)** Histogram of ω_d (Hz). **(C,D)** 2-D scatter diagram between ω_d (Hz) and H (cm) and FW (mg). r^2 means the square of Pearson's correlation coefficient. * $p < 0.05$, ** $p < 0.01$, and *** $p < 0.001$. Samples of **(A,C)** were grown in condition 1 and of **(B,D)** were grown in condition 2. These samples correspond to those used to calculate the values shown in **Table 3**. $n = 111$ [wild type in **(A,C)** in green], 41 [*nst1 nst3* in **(A,C)** in orange], 29 [wild type in **(B,D)** in blue], and 37 [*wrky12* in **(B,D)** in red].

Statistical Analyses

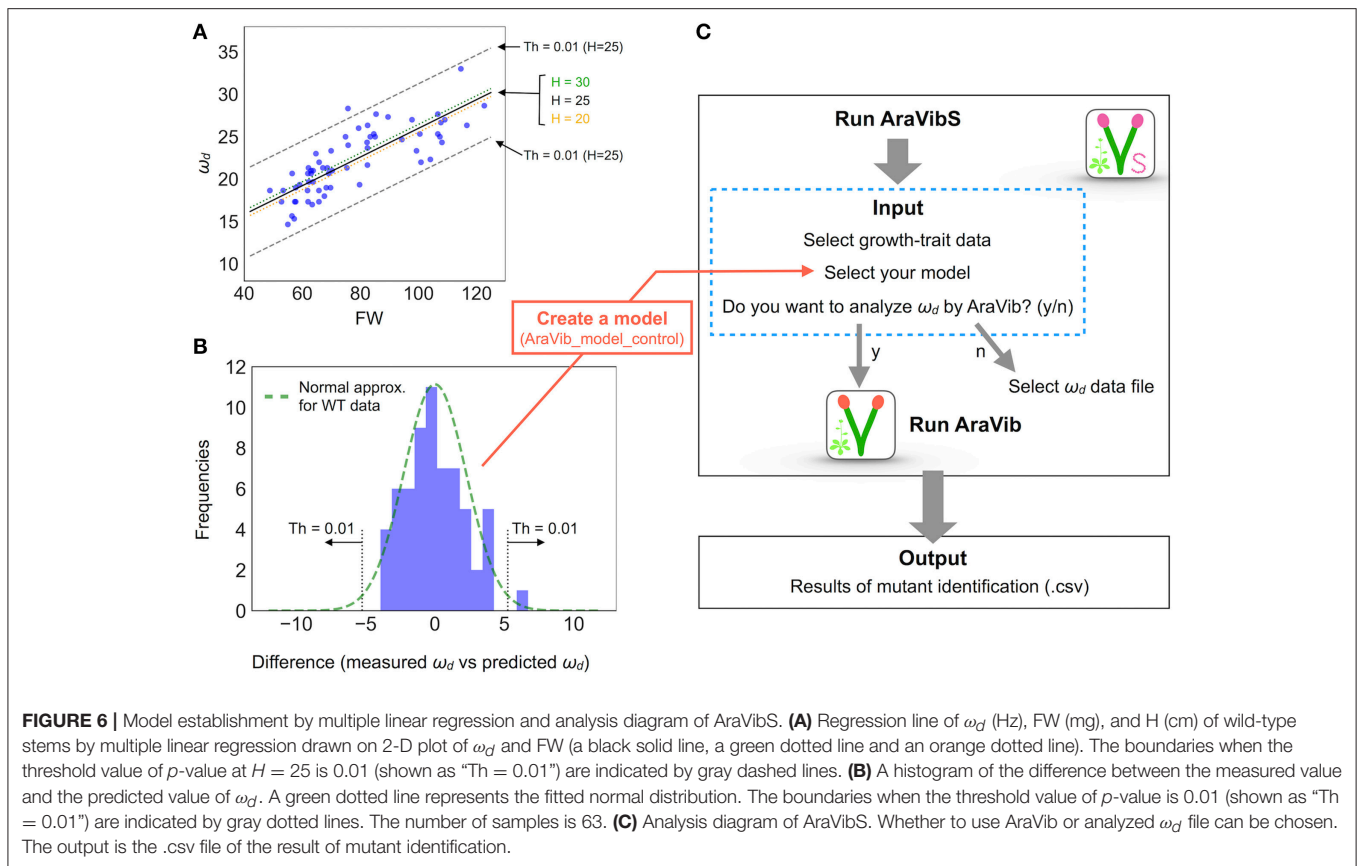
For individual parameters, the statistical functions of the Pandas, Numpy, and Scipy were used. Global scatter plots of all parameter pairs were drawn by the function of the Seaborn library. Histogram and scatter plots were drawn by the function of the pyplot package of the Matplotlib. For the statistical tests for differences, normality of data distribution (growth traits and oscillatory properties in each genotype and each growth condition) was tested using the Shapiro–Wilk Normality Test, and the homogeneity of variances was first analyzed with Bartlett's test. Normally distributed data with equal variances between two groups were examined using two-tailed Student's t -test. When the data was not normally distributed, a two-tailed Mann–Whitney U -test was used. The methods of multiple comparison test are shown in each table (**Tables 1, 2**).

Preparation of Alcohol-Insoluble Residues (AIRs)

To obtain AIRs, the red marker on the samples was wiped off after imaging of the stem vibration and the stem samples were soaked in 100% methanol for at least 1 d. The samples immersed in methanol were then treated sequentially with 100% acetone, methanol/chloroform (1:1) and 100% ethanol, and then dried overnight. AIRs of the samples were weighed with a precision balance.

Other Analyses

To calculate the initial angle, the images taken at the vibration start and after the vibration termination were merged. On the merged image, the angle was manually calculated by the function of ImageJ.



For the histological analysis, we prepared hand-cut sections of the 1.5-cm base portion of the stem and observed the brightfield and UV autofluorescence using an Axioskop2 fluorescent microscope (Carl-Zeiss Inc.). The cross-sectional area of the stem was measured by ImageJ.

RESULTS

Effect of the Initial Angle and the Number of Nodes on ω_d

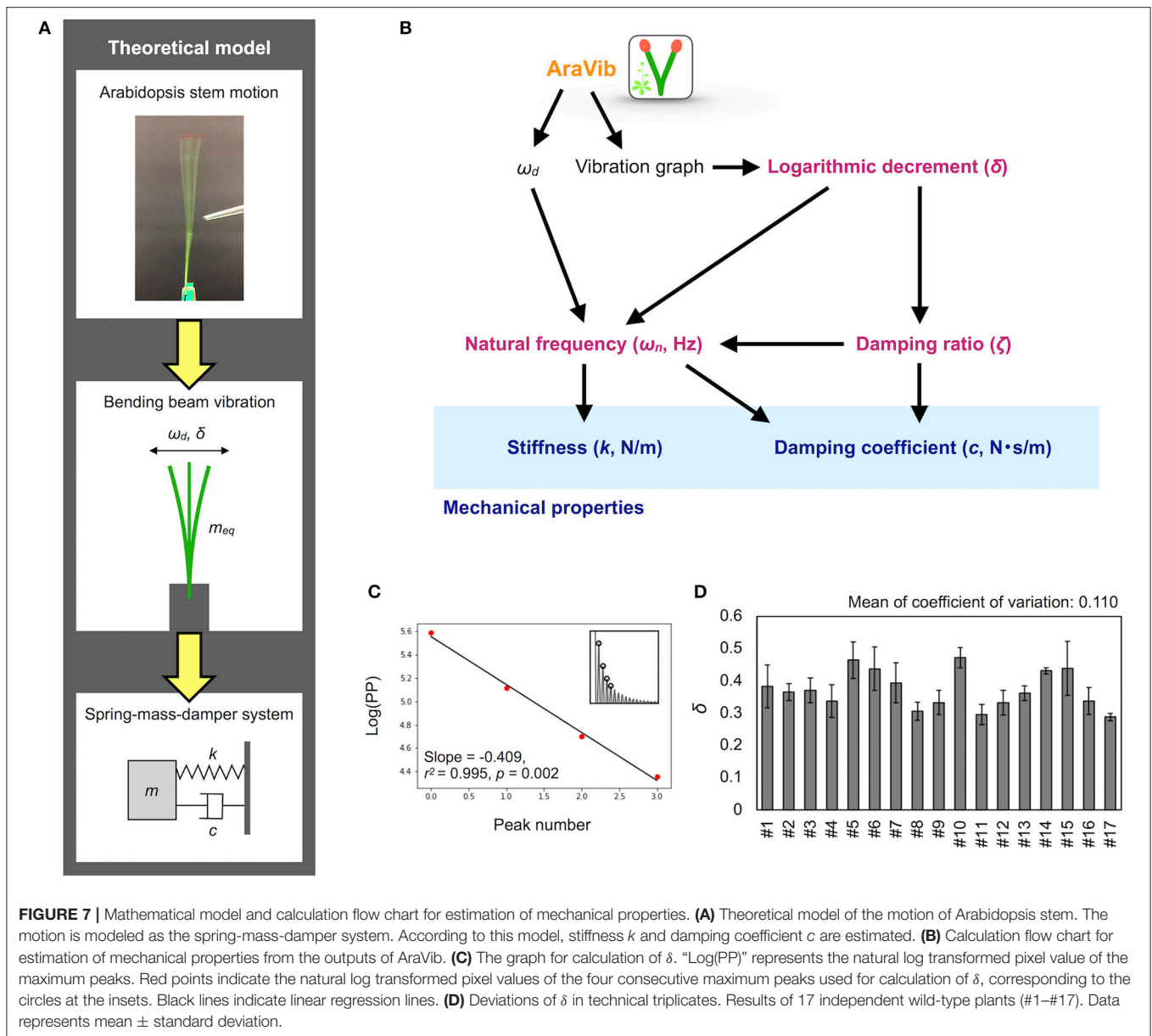
To calculate the ω_d , we developed the experimental method and the AraVib software to analyze the free vibrations of stems fixed at their basal ends. First of all, we investigated the magnitude of the technical variations of ω_d in the inflorescence stem of *A. thaliana* wild type. Technically triplicate experiments revealed that the variation of ω_d was only $\sim 1\%$ (Figure 4A). Next, we examined how the extent of the initial stem angle (shown in Figure 4B) affects ω_d . When the initial angle was roughly 20 to 30°, a typical waveform of damped oscillation was shown, while if the initial angle was $\sim 15^\circ$, an abnormal waveform was observed (Figure 4C). Nevertheless, experiments in which each sample was tested at multiple initial angles indicated that ω_d was nearly constant, regardless of the initial angle (Table 1). A previous study using the stem of *Equisetum hyemale* demonstrated the effect of nodes on stem vibration (Zajackowska et al., 2017). Therefore, we also examined the

effects of the numbers of nodes on ω_d in 10-cm stems of *A. thaliana*. We found that the number of nodes did not affect ω_d (Table 2).

Distribution of ω_d in Wild Type, *nst1 nst3*, and *wrky12*

Because the stem's stiffness affects ω_d in principle, we investigated whether the ω_d values in two cell-wall mutants differed from that of the wild type. These mutants were the *nst1 nst3* mutant in which the mechanical strength was reported to be weakened (Mitsuda et al., 2007) and the *wrky12* mutant in which the mechanical strength was presumed to be altered because of ectopic formation of the secondary cell walls (Wang et al., 2010). Examples of the vibration waveforms are shown in Figure 3B and Supplementary Figure 4, and the results of the multiple-sample analysis are shown in Table 3. The growth traits of the measured samples are shown in Supplementary Table 2.

The stem vibration waveform was a typical damped oscillation, regardless of genotype (Figure 3B and Supplementary Figure 4). However, the vibration of *nst1 nst3* was apparently slower (Supplementary Movies 1, 2, 5, 6), and the periods of the waves were larger than those of wild type (Figure 3B and Supplementary Figure 4). The major frequency, regarded as ω_d , of the *nst1 nst3* stems was lower than that of wild-type stems according to the FFT analysis (Figure 3B and Supplementary Figure 4). The mean of ω_d significantly



decreased to 34–36% of wild type in *nst1 nst3* (Table 3), and the distributions of the two genotypes were well separated (Figure 5A). However, no significant differences in the speed of vibration or the forms of the damped oscillation curves between wild type and *wrky12* were found, although the FFT analysis indicated that the frequency of the *wrky12* stem was slightly higher than that of the wild type stem (Figure 3B, Supplementary Figure 4, and Supplementary Movies 1, 2, 7, 8). The analysis of multiple samples revealed that ω_d was significantly increased to 115–120% of wild type in *wrky12* (Table 3), while the distributions of the two genotypes overlapped (Figure 5B). This result suggests that ω_d can be an indicator of changes in cell wall, which are accompanied by changes in stiffness.

Identifying Cell-Wall Mutants Using the Combination of ω_d and Growth Traits

ω_d showed a wide distribution in both wild type and *wrky12* mutants. It was assumed that the stiffness depended not only on the genotype but also on the degree of stem growth. To validate this assumption, we examined the correlation between ω_d and two growth traits, H and FW, in wild type, *nst1 nst3* and *wrky12*. In a two-dimensional (2-D) plot, ω_d showed a statistically significant positive correlation with H and FW under all conditions and in any genotype (Figures 5C,D). Thus, the stiffness also depends on the degree of the stem growth in *A. thaliana*.

The distribution of *wrky12* was well separated from that of the wild type on the 2-D plot of ω_d and growth traits (Figure 5D). Therefore, we hypothesized that cell-wall mutants could be distinguished from the wild type group using the correlation between ω_d and growth traits. Because ω_d was dependent on the degree of stem growth, an equation to obtain the expected value of ω_d from the H and FW values

was determined by a multiple linear regression (Figure 6A). The FW value contributed more to ω_d than the H value (Figure 6A). The 2-D plot suggested that the deviation from the regression equation of the wild type distribution fell within a certain range (Figure 6A). Based on the H and FW values, we calculated the expected value of ω_d from the regression equation and estimated the deviation from the measured value. The distribution of the deviation could be fitted to the normal distribution (Figure 6B). Using the fitted result as a model, we developed AraVibS, which combines AraVib with a program that classifies whether the sample is a mutant by determining the difference from wild type using the *p*-value (Figure 6C). When the *p*-value threshold of the model was set to 0.01 in each experimental condition, 100% of *nst1 nst3* samples were specified as mutant, while 60.0% of *wrky12* samples were specified as mutant (Table 4).

TABLE 1 | The effect of the initial angle on damped frequency and logarithmic decrement.

Angle (°)	Damped frequency ω_d (Hz)			Logarithmic decrement δ		
	Mean	sd	n	mean	sd	n
15	24.6	1.5	6	0.296 ^a	0.027	6
20	24.4	1.4	6	0.373 ^b	0.063	6
25	24.2	1.4	6	0.395 ^b	0.043	6
<i>p</i> -value	0.921			0.006		

Statistical differences (*p*-values) were calculated by a one-way ANOVA with repeated measures. The means between groups shown in a and b were significantly different by the pairwise comparisons with Holm's adjustment (*p* < 0.05).

TABLE 2 | The effect of the number of nodes on damped frequency and logarithmic decrement.

Nodes	Damped frequency ω_d (Hz)			Logarithmic decrement δ		
	Mean	sd	n	Mean	sd	n
1-2	24.2	3.1	7	0.354	0.095	6
3	24.8	2.4	11	0.397	0.060	11
4-5	24.8	2.4	7	0.340	0.040	6
<i>p</i> -value	0.976			0.233		

Statistical differences (*p*-values) were calculated by the Kruskal–Wallis H-test.

Quick Estimation of the Mechanical Properties From the AraVib Output

Using the AraVib output, we attempted to calculate *k* and *c*. As mentioned in the section Materials and Methods, *k* and *c* are calculated from ω_d and δ (Figures 7A,B). δ can be estimated from the vibration waveform (Figure 7C). As is for ω_d , technical variations of δ were investigated. The variation of δ was more than 10% in technical triplicates (Figure 7D). δ was consistent when the initial angle is in the range of 20 to 30° but tended to decrease when the initial angle was ~15° (Table 1, Figure 4C). The number of nodes had limited effects on δ (Table 2).

The estimated mechanical properties (*k* and *c*) are shown in Table 3, along with ω_n and ζ . The difference between ω_n and ω_d was ~1/10 Hz in both tested genotypes, which was below the frequency resolution (1/3 Hz) of ω_d . Thus, the ω_n and ω_d values were almost the same (Table 3). The

TABLE 3 | Oscillatory and mechanical properties of wild type and *wrky12* stems modeled as a vertically fixed and uniform prismatic beam without the oscillator.

Line	Condition	Damped natural frequency (ω_d , Hz)	Logarithmic decrement (d)	Damping ratio (ζ)	Natural frequency (ω_n , Hz)	Damping coefficient (<i>c</i> , $\times 10^{-4}$ N/[m/s])	Stiffness (<i>k</i> , N/m)	<i>n</i>
Wild type	1	20.5 ± 0.4 ^{#1}	0.300 ± 0.011	0.0474 ± 0.0017	20.6 ± 0.4	1.58 ± 0.09	0.227 ± 0.012	111
<i>nst1 nst3</i>		7.2 ± 0.2*	0.509 ± 0.017*	0.0808 ± 0.0027*	7.3 ± 0.2*	1.07 ± 0.07*	0.033 ± 0.003*	41
Wild type	2	24.2 ± 0.7	0.374 ± 0.021	0.0594 ± 0.0033	24.2 ± 0.7	3.63 ± 0.25	0.487 ± 0.032	29
<i>wrky12</i>		28.4 ± 0.6*	0.369 ± 0.017	0.0586 ± 0.0026	28.4 ± 0.6*	3.80 ± 0.25	0.599 ± 0.040 [†]	37

^{#1} Mean ± Standard Error, * Significant at *p* < 0.001 (Mann–Whitney U-test), [†] Significant at *p* < 0.05 (Welch's *t*-test).

TABLE 4 | The result of mutant detection by AraVibS.

Line	Condition	<i>n</i>	Specified as a mutant number (Ratio) ^{#1}	Difference ^{#2#3} (Hz)	<i>p</i> -values ^{#3}
Wild type	1	73	2 (2.7%)	−6.8 to 7.6 (0.0)	0.001–0.496 (0.293)
<i>nst1 nst3</i>		21	21 (100.0%)	−19.2 to −11.9 (−16.3)	0.000–0.000 (0.000)
Wild type	2	63	1 (1.6%)	−3.9 to 6.7 (−0.1)	0.001–0.493 (0.251)
<i>wrky12</i>		40	24 (60.0%)	1.0 to 10.8 (5.8)	0.000–0.334 (0.005)

^{#1} A model learned from wild type data of each condition is used for calculation. The threshold of *p*-value is 0.01. ^{#2} Difference = [measured ω_d] − [predicted ω_d]. ^{#3} Minimum–Maximum (Median).

k value was significantly reduced to 13–16% of wild type in *nst1 nst3* (Table 3), and the distribution was separated (Figure 8A). The c value was significantly lower in *nst1 nst3* (63–72% of wild type), but the distribution overlapped with that of wild type (Figure 8A). While the mean of c in *wrky12* was almost equivalent to that of wild type, the k value significantly increased to 115–131% of wild type (Table 3). The distribution of k overlapped between wild type and *wrky12* (Figure 8A).

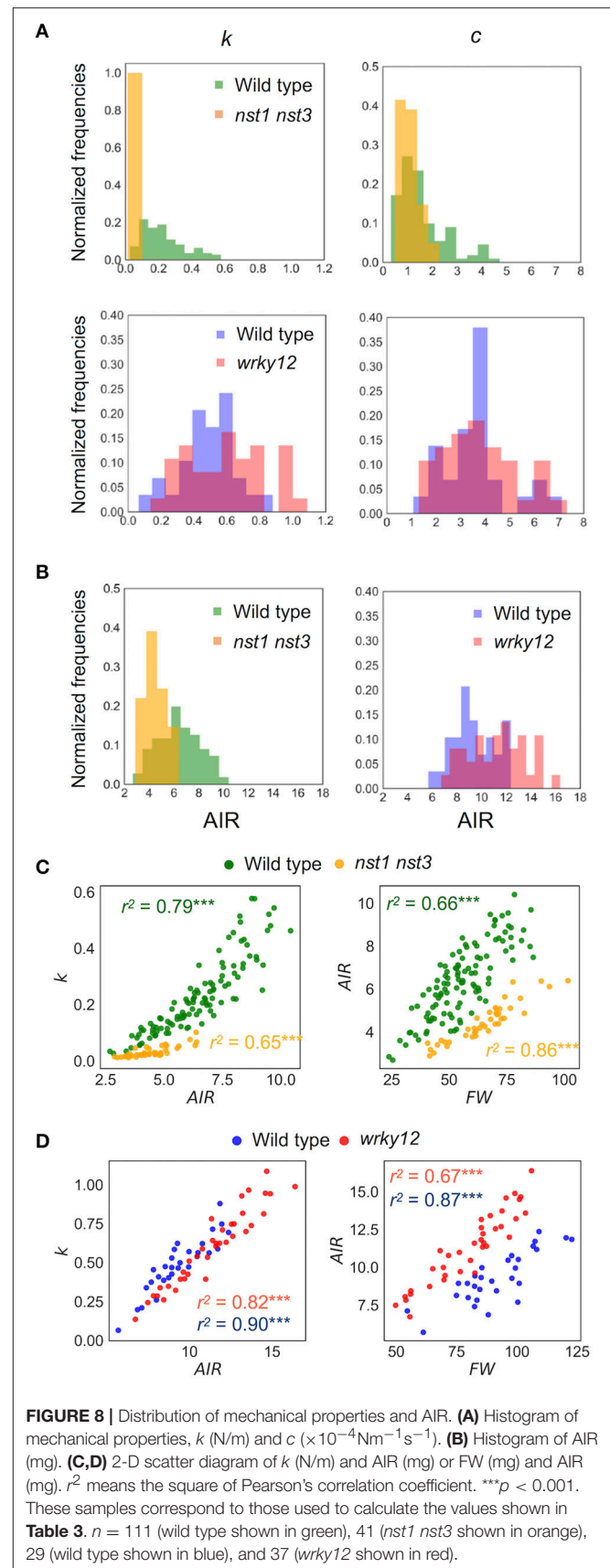
The Cell-Wall Density in the 10-cm Stem Was Well Correlated With k

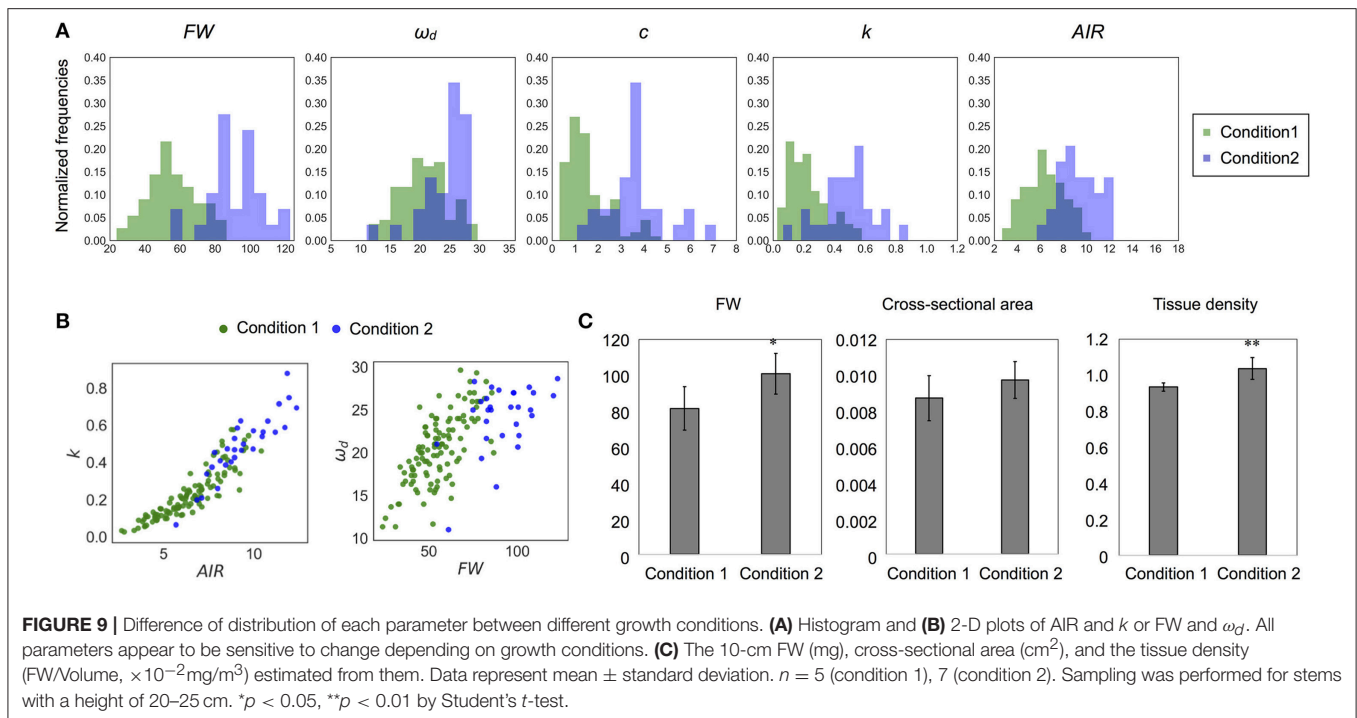
The k value drastically decreased in *nst1 nst3* and slightly increased in *wrky12* compared with wild type. In *nst1 nst3*, the amount of cell wall decreased because the secondary cell wall is absent (Mitsuda et al., 2007; Sakamoto and Mitsuda, 2015), whereas in *wrky12*, ectopic wood formation occurs in the pith (Wang et al., 2010) and the amount of cell wall is assumed to increase. Measurements revealed that the cell-wall density (AIR/FW) significantly decreased to 59–60% of wild type in *nst1 nst3* and significantly increased to 131–137% of wild type in *wrky12* under our experimental conditions (Figure 8B and Supplementary Table 2).

In the 2-D plot, a clear positive correlation between k and AIR was observed (Figures 8C,D). A regression analysis revealed the strong positive correlation between k and AIR (r^2 : wild type, 0.79 or 0.82; *nst1 nst3*, 0.65; *wrky12*, 0.90), which was comparable with the correlation between AIR and FW (r^2 : wild type, 0.66 or 0.67; *nst1 nst3*, 0.86; *wrky12*, 0.87). These results support a close relationship between the cell wall density and k .

Comparison of the ω_d and Mechanical Properties of Wild Type Populations Grown Under Different Conditions

There were differences in the distributions of ω_d and mechanical properties between wild-type samples grown under two conditions (Table 3, Figures 9A,B). In addition, the distributions of FW and AIR changed dramatically (Figures 9A,B and Supplementary Table 2). While wild type samples grown on the two conditions showed overlapping distributions on the 2-D plots of k and AIR, the distributions appeared different on the 2-D plots of ω_d and FW. To investigate the differences associated with these two growth conditions in more detail, we observed stem cross-sections. There was no obvious histological difference between the stems of plants grown under these two conditions (Supplementary Figure 9) nor were the cross-sectional stem areas significantly different (Figure 9C). The tissue densities estimated using FWs and the cross-sectional areas were significantly different between plants grown under the two conditions (Figure 9C). Thus, the FW, AIR, and tissue density of wild-type stems, as well as the ω_d and k values, differed between plants grown under the two conditions.





DISCUSSION

In this study, we developed a high-throughput analysis method for the free vibrations of *Arabidopsis* inflorescence stems that can identify cell-wall mutants with altered stiffness and quickly estimate mechanical properties. The AraVib software for free vibration analysis outputs a ω_d list for each analysis and three kinds of graphs for each sample. By analyzing ω_d and growth traits with AraVibS, 100% of *nst1 nst3* and 60% of *wrky12* samples were correctly judged as mutants. Furthermore, mechanical characteristics were estimated using ω_d and the graph of the vibration waveform.

Experiments with free vibration generally take a short time to capture vibrations that decay quickly. Because the time for data acquisition affects the analysis throughput, it is a fundamental advantage of the free-vibration method. However, this method uses one fixed end (termed the cantilever beam), unlike the free-free vibration method, and thus may not reflect the k level of the whole stem because various factors, including clamping effect, influence free vibrations. However, we concluded that our method is sufficient to estimate mechanical properties quickly for the investigation of genetic factors, because it was able to detect changes in the stem's stiffness of *Arabidopsis* mutants.

Another problem of measuring free vibration is that a high-speed camera or detector is required to obtain a sufficient resolution from the short-time displacement. Other studies of free vibration of plant stems used cameras with time resolutions of 200–1,000 fps (Der Loughian et al., 2014; Villibor et al., 2016; Zajczkowska et al., 2017). In this study,

we used high-speed shooting at 240 fps with the default function of an iPhone/iPad. According to the Nyquist–Shannon sampling theorem, for a frequency analysis without aliasing, the data sampling frequency must be more than twice the frequency of the measurement target (Nyquist, 1928; Shannon, 1949). Because the maximum ω_d of the 10-cm inflorescence stem of *A. thaliana* was 35 Hz, and the frame rate was more than 6.8 times the frequency, it was sufficient for the analysis.

The most important factor for the throughput of our method is the AraVib software. AraVib can analyze many videos in batches with only a few operations in the command line. Because Python knowledge is not necessary, researchers who are not familiar with computer programs and image analysis can easily use the software. The throughput rate is 30–40 s per sample, and all movies shot in a day are automatically analyzed by the batch process, which is essential for a large-scale screening. In vibrational analyses based on videos, coordinates are obtained by tracking a specified target. In previous studies, to capture stem vibrations, the features were tracked by an automatic analysis using the Kineplant-CR toolkit in MATLAB (Der Loughian et al., 2014), by a semi-automatic analysis with a free software for tracking (Zajczkowska et al., 2017) or by a manual analysis (Yazdanmanesh and Kalantari, 2015). In Spatz and Speck (2002), vibrations were captured by detecting tape, as a small marker, with the commercial software. Although it is not certain whether the image analysis was batch processed or ω_d was calculated seamlessly in these studies, the numbers of tested samples were relatively small and they did not appear to have high-throughput potential (Spatz and Speck, 2002; Der Loughian et al., 2014; Yazdanmanesh and

Kalantari, 2015; Zajaczkowska et al., 2017). Currently, the highest throughput method for determining free vibration uses a custom-made device rather than a camera (Zebrowski, 1991, 1999). Because this custom-made device includes a photodiode, amplifier and time-counter, it is not considered widely attainable for many biologists. In this study, more than 300 samples were analyzed, which is much more than in other studies using a camera. In addition, more than 50 samples could be analyzed in under 2 h. Therefore, this is the most high-throughput method compared with others available to many biologists.

We also developed AraVibS, which automatically detects mutants. As mentioned above, AraVibS was able to detect 100% of *nst1 nst3* and 60% of *wrky12* as mutants. AraVibS uses a multiple regression equation that calculates the expected value of ω_d from H and FW as a learned model, but it should be used carefully. Based on our analysis, the distributions of FW and ω_d changed even in the wild type population depending on growth conditions. This difference is likely caused by the differences in FW, AIR and tissue density. In fact, tissue density affects tissue strength (Niklas, 1993), which may result in changes in ω_d . When conducting mutant detection using AraVibS under new conditions, data from the wild type or control line should be analyzed under the same experimental conditions with AraVib_model_control.

Using ω_d and δ calculated from the output of AraVib, k and c were estimated according to the spring-mass-damper system model. The technical variation of ω_d was $\sim 1\%$ and was stable, independent of both the initial angle and the number of nodes. However, the variation of δ was $\sim 11\%$ in technical triplicates and was affected by the initial angle. For the calculation of k , the contribution of δ is very small, resulting in the estimated error of k being $\sim 2\%$. For the calculation of c , the contribution of δ is not ignorable, which results in an estimated error of c that is much larger than that of k . In *nst1 nst3*, based on the k value, stiffness was greatly decreased to $\sim 15\%$ of the wild type, which was consistent with our previous results in which the elastic modulus of *nst1 nst3* in the longitudinal direction was greatly reduced (Mitsuda et al., 2007; Yoshida et al., 2013). Thus, our method appears reliable enough to compare the k values of the stems of wild type and *nst1 nst3*. In addition, there was a difference in k between wild type and *wrky12*. Although the mechanical properties of *A. thaliana wrky12* stems have not been reported previously, there may be a difference in k between wild type and *wrky12*. Additionally, there was a difference in ω_d between wild type and *wrky12*. Considering that ω_n , which is almost the same value as ω_d , is inversely proportional to the square root of m_{eq} (Equation 7) and that k is strongly correlated with AIR, the vibrational analysis might be sensitive to changes in AIR/FW. However, more investigations will be needed to clarify this point.

A regression analysis revealed a strong and positive correlation between k and AIR. This strongly suggests that k may be closely related to the amount of components of secondary cell walls, which accounts for the majority of AIR. According to an analysis of wood, in the transverse direction,

hemicellulose and lignin are inferred to contribute to the elastic modulus (Salmén, 2004). In addition, the relationship between secondary cell wall components and stem's mechanical strength has been intensively studied using *A. thaliana*, poplar and tobacco. For example, a decrease in the total amount of lignin causes a decrease in k and increases the viscoelastic decay (Hepworth et al., 1998; Hepworth and Vincent, 1999; Köhler and Spatz, 2002; Koehler and Telewski, 2006; Özparpucu et al., 2017). Increasing the syringyl/guaiacyl ratio of lignin increases the modulus but does not change the bending stiffness (Koehler and Telewski, 2006). A decrease in xylan causes a decrease in wall thickness and causes a decrease in elastic modulus despite an increase in the relative amount of lignin (Li et al., 2011). However, an increase in the expression level of xyloglucanase increases the cellulose content and specific gravity, causing an increase in the elastic modulus (Park et al., 2004). Despite such intensive research, details regarding the relationship between cell wall components and mechanical properties remain unknown. A high-throughput method like ours enables the comprehensive investigation many genetic variations.

We demonstrated that our method is useful for the automatic detection of mutants and a quick estimation of mechanical properties. Among the existing screening methods used to evaluate the stem strength, visual observations can only detect drastic changes in strength, and the reliability of the hand-bending test strongly depends on the researcher's skill. Although the application of this method is not as rapid as visual observations or the hand-bending test, this is a robust, quantitative, and relatively sensitive method that does not require specific technical skills. The throughput rate of our method is comparable with or greater than that of screening by anatomical analysis with hand sectioning. Thus, we believe our method with further improvements will be suitable for large-scale screening studies.

AVAILABILITY

The GitHub page for the AraVib project is <https://github.com/MTNakata/AraVib>. The free Python packages or libraries, which are used in this study, are the OpenCV-Python package (<https://pypi.python.org/pypi/opencv-python>), NumPy package (<https://pypi.python.org/pypi/numpy>), the Python Pandas package (<https://pypi.python.org/pypi/pandas/0.18.1/>), SciPy library (<https://pypi.python.org/pypi/scipy>), the pyplot package of the Matplotlib (<https://pypi.python.org/pypi/matplotlib>), Scikit-learn package (<http://scikit-learn.org/stable/index.html>) and the Seaborn library (<https://pypi.python.org/pypi/seaborn>).

AUTHOR CONTRIBUTIONS

MN contributed to conception of the study, implemented AraVib and AraVibS, performed data collection and analysis, and wrote the initial draft of the manuscript. MN and MT contributed to the design of AraVib and AraVibS. MN, MT, and KY contributed to interpretation of data. MN, MT, SS, and NM contributed to the design of the laboratory experiments. MN, MT, KY, and

NM contributed to manuscript revision. All authors read and approved the submitted version.

ACKNOWLEDGMENTS

We thank A. Hosaka, M. Yamada, and Y. Sugimoto for technical support. This study was performed under the support of JST ALCA program (to NM). We thank Lesley Benyon, Ph.D.

REFERENCES

- Abramoff, M. D., Magalhães, P. J., and Ram, S. J. (2004). Image processing with ImageJ. *Biophotonics Int.* 11, 36–42.
- Braybrook, S. A., and Peaucelle, A. (2013). Mechano-chemical aspects of organ formation in *Arabidopsis thaliana*: the relationship between auxin and pectin. *PLoS ONE* 8:e57813. doi: 10.1371/journal.pone.0057813
- Brulé, V., Rafsanjani, A., Pasini, D., and Western, T. L. (2016). Hierarchies of plant stiffness. *Plant Sci.* 250, 79–96. doi: 10.1016/j.plantsci.2016.06.002
- Burström, H. G. (1971). Tissue tensions during cell elongation in wheat roots and a comparison with contractile roots. *Physiol. Plant.* 25, 509–513. doi: 10.1111/j.1399-3054.1971.tb01481.x
- Burström, H. G., Uhrström, I., and Olausson, B. (1970). Influence of auxin on Young's modulus in stems and roots of Pisum and the theory of changing the modulus in tissues. *Physiol. Plant.* 23, 1223–1233. doi: 10.1111/j.1399-3054.1970.tb08898.x
- Burström, H. G., Uhrström, I., and Wurscher, R. (1967). Growth, turgor, water potential, and Young's modulus in pea internodes. *Physiol. Plant.* 20, 213–231. doi: 10.1111/j.1399-3054.1967.tb07157.x
- Cassan-Wang, H., Goué, N., Saidi, M. N., Legay, S., Sivadon, P., Goffner, D., et al. (2013). Identification of novel transcription factors regulating secondary cell wall formation in Arabidopsis. *Front. Plant Sci.* 4:189. doi: 10.3389/fpls.2013.00189
- Cosgrove, D. J., and Green, P. B. (1979). Rapid suppression of growth by blue light: BIOPHYSICAL MECHANISM OF ACTION. *Plant Physiol.* 68, 1447–1453.
- de Silva, C. W. (2006). *Vibration: Fundamentals and Practice, 2nd Edn.* Boca Raton, FL: CRC Press.
- Der Loughian, C., Tadrast, L., Allain, J. M., Diener, J., Moulia, B., and De Langre, E. (2014). Measuring local and global vibration modes in model plants. *Comptes Rendus Mec.* 342, 1–7. doi: 10.1016/j.crme.2013.10.010
- Falk, S., Hertz, C. H., and Virgin, H. I. (1958). On the relation between turgor pressure and tissue rigidity. I. *Physiol. Plant.* 11, 802–817. doi: 10.1111/j.1399-3054.1958.tb02874.x
- Fernandes, A. N., Chen, X., Scotchford, C. A., Walker, J., Wells, D. M., Roberts, C. J., et al. (2012). Mechanical properties of epidermal cells of whole living roots of *Arabidopsis thaliana*: an atomic force microscopy study. *Phys. Rev. E Stat. Nonlinear Soft Matter Phys.* 85(2 Pt 1):21916. doi: 10.1103/PhysRevE.85.021916
- Finney, E. E., and Abbott, J. A. (1979). Methods for testing the dynamic mechanical response of solid foods. *J. Food Qual.* 2, 55–74. doi: 10.1111/j.1745-4557.1979.tb00658.x
- Gibson, L. J. (2012). The hierarchical structure and mechanics of plant materials. *J. R. Soc. Interface* 9, 2749–2766. doi: 10.1098/rsif.2012.0341
- Halabe, U. B., Bidigalu, G. M., GangaRao, H. V. S., and Ross, R. J. (1997). Nondestructive evaluation of green wood using stress wave and transverse vibration techniques. *Mater. Eval.* 55, 1013–1018.
- Harris, F. J. (1978). (1999). On the use of windows for harmonic analysis with the discrete Fourier transform. *Proc. IEEE* 66, 51–83. doi: 10.1109/PROC.1978.10837
- Hepworth, D. G., and Vincent, J. F. V. (1999). The growth response of the stems of genetically modified tobacco plants (*Nicotiana tabacum* 'Samsun') to flexural stimulation. *Ann. Bot.* 83, 39–43.
- Hepworth, D. G., Vincent, J. F. V., and Schuch, W. (1998). Using viscoelastic properties of the woody tissue from tobacco plants (*Nicotiana tabacum*) to comment on the molecular structure of cell walls. *Ann. Bot.* 81, 729–734. doi: 10.1006/anbo.1998.0619

from Edanz Group (www.edanzediting.com/ac) for language editing.

SUPPLEMENTARY MATERIAL

The Supplementary Material for this article can be found online at: <https://www.frontiersin.org/articles/10.3389/fpls.2018.00780/full#supplementary-material>

- Köhler, L., and Spatz, H. C. (2002). Micromechanics of plant tissues beyond the linear-elastic range. *Planta* 215, 33–40. doi: 10.1007/s00425-001-0718-9
- Koehler, L., and Telewski, F. W. (2006). Biomechanics and transgenic wood. *Am. J. Bot.* 93, 1433–1438. doi: 10.3732/ajb.93.10.1433
- Li, Q., Min, D., Wang, J. P., Peszlen, I., Horvath, L., Horvath, B., et al. (2011). Down-regulation of glycosyltransferase 8D genes in *Populus trichocarpa* caused reduced mechanical strength and xylan content in wood. *Tree Physiol.* 31, 226–236. doi: 10.1093/treephys/tpr008
- MacMillan, C. P., O'Donnell, P. J., Smit, A., Evans, C. R., and Stachurski, Z. H. (2013). A survey of the natural variation in biomechanical and cell wall properties in inflorescence stems reveals new insights into the utility of Arabidopsis as a wood model. *Funct. Plant Biol.* 40, 662–676. doi: 10.1071/FP12386
- Mitsuda, N., Iwase, A., Yamamoto, H., Yoshida, M., Seki, M., Shinozaki, K., et al. (2007). NAC transcription factors, NST1 and NST3, are key regulators of the formation of secondary walls in woody tissues of Arabidopsis. *Plant Cell* 19, 270–280. doi: 10.1105/tpc.106.047043
- Mott, L., Shaler, S. M., and Groom, L. H. (1996). A Technique to measure strain distributions in single wood pulp fibers. *Wood Fiber Sci.* 4, 429–437.
- Niklas, K. J. (1993). Influence of tissue density-specific mechanical properties on the scaling of plant height. *Ann. Bot.* 72, 173–179. doi: 10.1006/anbo.1993.1096
- Niklas, K. J., and Moon, F. C. (1988). Flexural stiffness and modulus of elasticity of flower stalks from allium stalks from allium sativum as measured by multiple resonance frequency spectra. *Am. J. Bot.* 75, 1517–1525. doi: 10.1002/j.1537-2197.1988.tb11225.x
- Nyquist, H. (1928). Certain topics in telegraph transmission theory. *Am. Instit. Electric. Eng. Trans.* 47, 617–644. doi: 10.1109/T-AIEE.1928.5055024
- Özparpucu, M., Rüggeberg, M., Gierlinger, N., Cesarino, I., Vanholme, R., Boerjan, W., et al. (2017). Unravelling the impact of lignin on cell wall mechanics: a comprehensive study on young poplar trees downregulated for CINNAMYL ALCOHOL DEHYDROGENASE (CAD). *Plant J.* 91, 480–490. doi: 10.1111/tjp.13584
- Park, Y. W., Baba, K., Furuta, Y., Iida, I., Sameshima, K., Arai, M., et al. (2004). Enhancement of growth and cellulose accumulation by overexpression of xyloglucanase in poplar. *FEBS Lett.* 564, 183–187. doi: 10.1016/S0014-5793(04)00346-1
- Peaucelle, A. (2014). AFM-based mapping of the elastic properties of cell walls: at tissue, cellular, and subcellular resolutions. *J. Vis. Exp.* 89:51317. doi: 10.3791/51317
- Peaucelle, A., Braybrook, S. A., Le Guillou, L., Bron, E., Kuhlemeier, C., and Höfte, H. (2011). Pectin-induced changes in cell wall mechanics underlie organ initiation in arabidopsis. *Curr. Biol.* 21, 1720–1726. doi: 10.1016/j.cub.2011.08.057
- Radotić, K., Roduit, C., Simonović, J., Hornitschek, P., Fankhauser, C., Mutavdžić, D., et al. (2012). Atomic force microscopy stiffness tomography on living *Arabidopsis thaliana* cells reveals the mechanical properties of surface and deep cell-wall layers during growth. *Biophys. J.* 103, 386–394. doi: 10.1016/j.bpj.2012.06.046
- Ryden, P., Sugimoto-Shirasu, K., Smith, A. C., Findlay, K., Reiter, W. D., and McCann, M. (2003). Tensile properties of Arabidopsis cell walls depend on both a xyloglucan cross-linked microfibrillar network and rhamnogalacturonan II-borate complexes. *Plant Physiol.* 132, 1033–1040. doi: 10.1104/pp.103.021873
- Sakamoto, S., and Mitsuda, N. (2015). Reconstitution of a secondary cell wall in a secondary cell wall-deficient Arabidopsis mutant. *Plant Cell Physiol.* 56, 299–310. doi: 10.1093/pcp/pcu208

- Sakamoto, S., Takata, N., Oshima, Y., Yoshida, K., Taniguchi, T., and Mitsuda, N. (2016). Wood reinforcement of poplar by rice NAC transcription factor. *Sci. Rep.* 6:19925. doi: 10.1038/srep19925
- Salmén, L. (2004). Micromechanical understanding of the cell-wall structure. *C. R. Biol.* 327, 873–880. doi: 10.1016/j.crvi.2004.03.010
- Santoro, N., Cantu, S., Tornqvist, C., Falbel, T. G., Bolivar, J. L., Patterson, S. E., et al. (2010). A high-throughput platform for screening milligram quantities of plant biomass for lignocellulose digestibility. *Bioener. Res.* 3, 93–102. doi: 10.1007/s12155-009-9074-6
- Shah, D. U., Reynolds, T. P. S., and Ramage, M. H. (2017). The strength of plants: theory and experimental methods to measure the mechanical properties of stems. *J. Exp. Bot.* 68, 4497–4516. doi: 10.1093/jxb/erx245
- Shannon, C. E. (1949). Communication in the presence of noise. *Proc. IRE* 37, 10–21. doi: 10.1109/JRPROC.1949.232969
- Spatz, H. C., and Speck, O. (2002). Oscillation frequencies of tapered plant stems. *Am. J. Bot.* 89, 1–11. doi: 10.3732/ajb.89.1.1
- Uhrström, I. (1969). The time effect of auxin and calcium on growth and elastic modulus in hypocotyls. *Physiol. Plant.* 22, 271–287. doi: 10.1111/j.1399-3054.1969.tb07376.x
- Uhrström, I., and Svensson, S. (1979). The effect of coumarin on Young's modulus in sunflower stems and maize roots and on water permeability in potato parenchyma. *Physiol. Plant.* 45, 41–44. doi: 10.1111/j.1399-3054.1979.tb01660.x
- Villibor, G. P., Santos, F. L., de Queiroz, D. M., Khoury J. K. Jr., and de Carvalho Pinto, F. A. (2016). Determination of modal properties of the coffee fruit-stem system using high speed digital video and digital image processing. *Acta Sci.* 38, 41–48. doi: 10.4025/actascitechnol.v38i1.27344
- Virgin, H. I. (1955). A new method for the determination of the turgor of plant tissues. *Physiol. Plant.* 8, 954–962. doi: 10.1111/j.1399-3054.1955.tb07791.x
- Wang, H., Avci, U., Nakashima, J., Hahn, M. G., Chen, F., and Dixon, R. A. (2010). Mutation of WRKY transcription factors initiates pith secondary wall formation and increases stem biomass in dicotyledonous plants. *Proc. Natl. Acad. Sci. U. S. A.* 107, 22338–22343. doi: 10.1073/pnas.1016436107
- Yamamoto, H., Iwamoto, M., and Haginuma, S. (1980). Acoustic impulse response method for measuring natural frequency of intact fruits and preliminary applications to internal quality evaluation of apples and watermelons. *J. Texture Stud.* 11, 117–136. doi: 10.1111/j.1745-4603.1980.tb00312.x
- Yazdanmanesh, A., and Kalantari, D. (2015). Investigation of vibrational properties of apple, lemon and orange branches under dynamic loads. *Int. J. Eng. Appl. Sci.* 2:19.
- Yoshida, K., Sakamoto, S., Kawai, T., Kobayashi, Y., Sato, K., Ichinose, Y., et al. (2013). Engineering the *Oryza sativa* cell wall with rice NAC transcription factors regulating secondary wall formation. *Front. Plant Sci.* 4:383. doi: 10.3389/fpls.2013.00383
- Zajaczkowska, U., Kucharski, S., Nowak, Z., and Grabowska, K. (2017). Morphometric and mechanical characteristics of *Equisetum hyemale* stem enhance its vibration. *Planta* 245, 835–848. doi: 10.1007/s00425-017-2648-1
- Zebrowski, J. (1991). The use of free vibrations to measure peduncle stiffness in triticale. *J. Exper. Bot.* 42, 1207–1212. doi: 10.1093/jxb/42.9.1207
- Zebrowski, J. (1999). Dynamic behaviour of inflorescence-bearing Triticale and Triticum stems. *Planta* 207, 410–417. doi: 10.1007/s004250050499
- Zhong, R., Richardson, E. A., and Ye, Z. H. (2007). Two NAC domain transcription factors, SND1 and NST1, function redundantly in regulation of secondary wall synthesis in fibers of Arabidopsis. *Planta* 225, 1603–1611. doi: 10.1007/s00425-007-0498-y

Conflict of Interest Statement: KY is employed by Taisei Corporation.

The remaining authors declare that the research was conducted in the absence of any commercial or financial relationships that could be construed as a potential conflict of interest.

Copyright © 2018 Nakata, Takahara, Sakamoto, Yoshida and Mitsuda. This is an open-access article distributed under the terms of the Creative Commons Attribution License (CC BY). The use, distribution or reproduction in other forums is permitted, provided the original author(s) and the copyright owner are credited and that the original publication in this journal is cited, in accordance with accepted academic practice. No use, distribution or reproduction is permitted which does not comply with these terms.